Available online at www.sciencedirect.com
SCIENCE DIRECT®
Journal of Chromatography A, 1078 (2005) 98–112
JOURNAL OF CHROMATOGRAPHY A
www.elsevier.com/locate/chroma

Characterization of a peptide affinity support that binds selectively to staphylococcal enterotoxin B

Guangquan Wang [1], Ruben G. Carbonell *

Department of Chemical and Biomolecular Engineering, North Carolina State University, 1017 Main Campus Drive, Centennial Campus, Partner's Building I, Suite 3200, Box 7006, Raleigh, NC 27695-7006, USA

Received 8 February 2005; received in revised form 28 April 2005; accepted 2 May 2005

Abstract

The influences of mass transfer and adsorption–desorption kinetics on the binding of staphylococcal enterotoxin B (SEB) to an affinity resin with the peptide ligand, Tyr-Tyr-Trp-Leu-His-His (YYWLHH) have been studied. The bed and particle porosities, the axial dispersion coefficient and the pore diffusivity were measured using pulse experiments under unretained conditions. Adsorption isotherms for SEB on YYWLHH resins with peptide densities in the range from 6 to 220 μmol/g were measured and fitted to a bi-Langmuir equation. At peptide densities below 9 μmol/g and above 50 μmol/g, dissociation constants were lower (2×10^{-3} to 7×10^{-3} mol/m^3), and binding capacities were larger (43–47 mg SEB/g). In the range from 9 to 50 μmol/g dissociation constants were larger (13×10^{-3} to 24×10^{-3} mol/m^3) and capacities were lower (33–37 mg SEB/g). These observations are consistent with a transition from single point attachment of the protein to the ligand at low peptide densities to multipoint attachment at high peptide densities. The general rate (GR) model of chromatography was used to fit experimental breakthrough curves under retained conditions to determine the intrinsic rate constants for adsorption, which varied from 0.13 to 0.50 m^3 mol^{-1} s^{-1}, and exhibited no clear trend with increasing peptide density. An analysis of the number of transfer units for the various mass transfer steps in the column indicated that film mass transfer, pore diffusion (POR) and the kinetics of adsorption can all play an important role in the overall rate of adsorption, with the intrinsic adsorption step apparently being the rate determining step at peptide densities below 50 μmol/g.

Keywords: Mathematical modeling; Peptide affinity chromatography; Peptide density; Staphylococcal enterotoxin B

1. Introduction

Short peptides have been used as affinity ligands to purify various proteins [1–6]. It has been shown that short peptides are more specific than pseudo affinity ligands such as dye ligands and metal ions, and more stable than bioaffinity ligands such as antibodies [2,4]. Peptide ligands used in affinity chromatography to isolate or concentrate a target protein are generally screened from solid phase combinatorial or parallel peptide libraries, which are created on a suitable chromatographic support [7]. The relatively high selectivity, stability, and low cost of small peptides make them suitable as affinity ligands to purify proteins in large-scale purification processes [4]. Little information is available in the literature on the role of mass transfer and adsorption–desorption kinetics in peptide affinity chromatography. Such information is important for column design and optimization. A lumped kinetic model has been employed to fit the breakthrough curves of fibrinogen that binds to a short peptide FLLVPL [6]. However, the capacity and association constant derived from the fitting of the experimental breakthrough data with this model is inconsistent with equilibrium experiments. The use of too simple a mass transfer model might lead to erroneous descriptions of the experimental data and to misunderstandings of the fundamentals of the process involved [8]. A more com-

* Corresponding author. Tel.: +1 919 515 5118; fax: +1 919 515 5831.
E-mail address: ruben@ncsu.edu (R.G. Carbonell).
[1] Present address: Bayer HealthCare LLC, Technology Department, 8368 US 70 West, P.O. Box 507, Clayton, NC 27520, USA.

0021-9673/$ – see front matter © 2005 Published by Elsevier B.V.
doi:10.1016/j.chroma.2005.05.010

plete model that accounts for all mass transfer resistances and adsorption–desorption kinetics should be used to model the breakthrough curves or zone profiles.

Another factor that is crucial for column design and optimization is the peptide density on the adsorbent. Ligand density has significant influences on the interactions between the peptide ligands and the target protein. A better understanding of these effects can help to optimize the affinity adsorption of the target protein to increase the binding efficiency. If the binding is attributed to monovalent interactions, the capacity increases with increase in ligand density, while the association constant may remain constant at low ligand density and decrease at high ligand density due to steric effects. Such an effect was seen on the binding of s-protein to YNFEVL. Thus, there is an optimal density at which the peptide ligands have high capacity and an acceptable extent of steric hindrance. Small protein molecules, such as s-protein, have monovalent interactions with peptide ligands and typically show the phenomena mentioned above [4]. If the binding is attributed to multivalent interactions, increasing the ligand density typically increases the capacity and association constant. This was seen in the adsorption of a large protein molecule, von Willebrand factor (vWF), to peptide ligands on a resin surface [5]. But for highly specific ligands, increasing the ligand density tends to increase the steric hindrance at the surface and makes the binding less efficient, decreasing the association constant and the ligand utilization.

Staphylococcal enterotoxin B (SEB) is a primary toxin in food poisoning, which can cause emesis as a gastrointestinal toxin. In addition, it functions as a superantigen to interact with the major histocompatibility complex class II molecules (MHCII) and T cells bearing particular Vβ elements, triggering a massive release of T cell-derived cytokines followed by allergic and autoimmune symptoms [9,10]. The legal dose capable of incapacitating 50% of the exposed human population (LD_{50}) is 0.02 μg/kg by the inhalational route [11]. A short peptide ligand that selectively binds to SEB, YYWLHH, has been identified from a solid phase combinatorial peptide library [12]. Mass transfer parameters and intrinsic rate constants are required for the design of peptide affinity columns that can be used to either detect or remove SEB from solution. In this article, a description of the mass transfer and adsorption–desorption kinetics in peptide affinity chromatography is presented using SEB as a model protein. The apparent heterogeneous nature of the binding of SEB to YYWLHH resin is described by a bi-Langmuir isotherm. A complete chromatography model, the general rate (GR) model, is employed to model the breakthrough curves of SEB with mass transfer parameters determined from pulse experiments. The rate-limiting steps are determined from an analysis of the number of transfer units. Results of the GR model are compared to those of several simpler models, such as the lumped pore diffusion (POR) model, the transport-dispersive (TD) model, and the reaction-dispersive (RD) model, to help understand the role of each process involved in peptide affinity chromatography. The effect of peptide density on the dissociation constant, maximum capacity, and rate constant for adsorption provides information on the mechanism of SEB adsorption to the YYWLHH support.

2. Theory

2.1. Isotherm models

The Langmuir model has been used to fit adsorption isotherm data of proteins on peptide resins [4–6]. It assumes a set of equivalent, distinguishable and independent binding sites [13]. However, the adsorption of protein molecules onto peptide ligands might involve multi-point binding, and can be affected by non-homogeneous local peptide density distributions. As a result, a more complex isotherm equation may need to be used to provide a more accurate fit to the experimental data. For example, Bastek [14] found that a bi-Langmuir model improved the fit of isotherms for binding α_1-proteinase inhibitor (α_1PI) to peptide resins. The bi-Langmuir model postulates two independent binding sites, a high-energy binding site and a low-energy binding site. The bi-Langmuir equations are written in the form,

$$Q^* = \frac{Q^*_{m,1} C}{K_{d,1} + C} + \frac{Q^*_{m,2} C}{K_{d,2} + C} \quad (1)$$

where K_d and Q^*_m are the dissociation constant and the maximum capacity, respectively.

2.2. General rate model

The GR model [8,13,15] takes into account all mass transfer processes in packed bed chromatography, namely (1) axial dispersion of the solute molecules in the bulk phase; (2) film mass transfer of the solute molecules from the bulk phase to the external surface of the adsorbent particles; (3) diffusion of the solute molecules inside the pores of these particles; and (4) rates of adsorption and desorption on the pore surface. One of the challenging tasks of the GR model is the independent determination of a relatively large number of mass transfer parameters. Due to the mathematical complexity of the GR model, only numerical solutions are available.

In this particular application of the GR model, we have made the following assumptions: (1) the chromatographic process is isothermal; (2) the column is packed homogeneously with porous particles that are spherical and uniform in size; (3) the mobile phase velocity is constant, and there is no convection inside the pores; (4) the compressibility of the mobile phase is negligible; (5) the radial concentration gradient in the column is negligible; (6) convection and axial dispersion are the only mass transfer mechanisms in the axial direction, and the dispersion coefficient is independent of the concentration; (7) the surface of each particle is assumed to be uniform; (8) surface diffusion within the particles is neglected. The GR model in dimensionless form consists of the

following differential equations for solute continuity in the fluid and particle phase,

$$\frac{\partial c_b}{\partial \tau} - \frac{1}{Pe}\frac{\partial^2 c_b}{\partial z^2} + \frac{\partial c_b}{\partial z} + \xi(c_b - c_p|_{r=1}) = 0 \quad (2)$$

$$(1-\varepsilon_p)\frac{\partial q}{\partial \tau} + \varepsilon_p \frac{\partial c_p}{\partial \tau} - \eta\left(\frac{1}{r^2}\frac{\partial}{\partial r}\left(r^2\frac{\partial c_p}{\partial r}\right)\right) = 0 \quad (3)$$

All dimensionless groups are defined in the nomenclature section. As demonstrated later, the isotherm data of SEB on short peptide ligands (YYWLHH) fits very well to the bi-Langmuir isotherm. Thus we assume there are two types of independent binding sites, type I and type II, and that the adsorption rate of SEB is of second order while the desorption rate is first order on each site,

$$q = q_1 + q_2 \quad (4)$$

$$\frac{\partial q_1}{\partial \tau} = Da_1^a c_p(q_{m,1}^* - q_1) - Da_1^d q_1 \quad (5)$$

$$\frac{\partial q_2}{\partial \tau} = Da_2^a c_p(q_{m,2}^* - q_2) - Da_2^d q_2 \quad (6)$$

Under conditions of local equilibrium, setting the time derivatives in Eqs. (5) and (6) to zero results in the bi-Langmuir isotherm,

$$q_1^* = \frac{a_1 c_p}{1 + b_1 c_p} \quad (7)$$

$$q_2^* = \frac{a_2 c_p}{1 + b_2 c_p} \quad (8)$$

The initial conditions are

$$\tau = 0, c_b = 0; \quad (9)$$

$$c_p = 0; \quad (10)$$

$$q = 0; \quad (11)$$

$$q_1 = 0; \quad (12)$$

$$q_2 = 0 \quad (13)$$

At the entrance and exit of the column the boundary conditions for the fluid phase equation are of the Danckwerts form [16],

$$z = 0, \frac{\partial c_b}{\partial z} = Pe_b(c_b - 1); \quad (14)$$

$$z = 1, \frac{\partial c_b}{\partial z} = 0 \quad (15)$$

The boundary conditions for the intraparticle diffusion equation include convective diffusion at the particle surface,

$$r = 0, \frac{\partial c_p}{\partial r} = 0; \quad (16)$$

$$r = 1, \frac{\partial c_p}{\partial r} = Bi(c_b - c_p|_{r=1}) \quad (17)$$

A Matlab code was written to solve the GR model equations. The finite element method was used to discretize the bulk phase partial differential equation [15] while the orthogonal collocation method was used to discretize the pore phase partial differential equation [17,18]. The resulting ordinary partial differential equations were solved using the built-in function *ode15s* in Matlab. All mass transfer parameters were either measured independently or estimated from correlations, and all isotherm parameters were determined experimentally. The intrinsic rate constants for adsorption were then estimated by fitting the breakthrough curve using the built-in function *lsqcurvefit* in Matlab. The desorption rate constants were then evaluated using the relation between the adsorption equilibrium constant and the ratio of the adsorption to desorption rate constants.

2.3. Estimation of mass transfer parameters

Both the interstitial porosity (ε_b) of the column and the particle porosity (ε_p) need to be determined before the estimation of other mass transfer parameters. For a pulse of solute that is not retained in the column and can access all the pores in the chromatographic support, the total porosity (ε_t) is related to the first moment (μ_1) of the elution profiles [19–21],

$$\mu_1 = \frac{\int_0^\infty C(L,t)t\,dt}{\int_0^\infty C(L,t)\,dt} = \frac{L}{u_0}\varepsilon_t \quad (18)$$

where the total porosity includes contributions from both the bed and particle porosities,

$$\varepsilon_t = \varepsilon_b + (1-\varepsilon_b)\varepsilon_p \quad (19)$$

A plot of μ_1 versus L/u_0 should give a straight line, whose slope is the total porosity. If a large solute that is excluded from particle pores is used in the pulse injections, the total porosity measured in this case is only the interstitial porosity of the column (ε_b). The particle porosity can be then calculated using Eq. (19). As described in the experimental section, the bed porosity was determined using pulses of blue dextran in a column filled with particles of the same size as the affinity resin but much smaller pore size. The intraparticle porosity was determined from the first moment of pulses of SEB in a column filled with resin without peptide that did not retain the protein.

The film mass transfer coefficient (k_f) can be estimated using the correlation of Wakao et al. [22],

$$Sh = 2 + 1.45\,Re^{1/2}Sc^{1/3} \quad (20)$$

The axial dispersion coefficient (D_b) and the pore diffusivity (D_p) can be determined from the height equivalent to a theoretical plate (HETP) under unretained conditions if the outlet pulse profile is a Gaussian peak in a pulse experiment [19–21]. In the GR model, the HETP equation for an unretained solute is related to the moments of the pulse response and the column length,

$$\text{HETP} = \frac{\mu_2^* L}{\mu_1^2} = \frac{2\varepsilon_b D_b}{u_0} + \frac{2\varepsilon_p^2(1-\varepsilon_b)R_p^2}{15[\varepsilon_b + (1-\varepsilon_b)\varepsilon_p]^2} \times \left(\frac{1}{\varepsilon_p D_p} + \frac{5}{k_f R_p}\right) u_0 \quad (21)$$

The contribution of film mass transfer to the HETP is calculated using the estimated film mass transfer coefficient from Eq. (20),

$$\text{HETP}_f = \frac{2\varepsilon_p^2(1-\varepsilon_b)R_p u_0}{3k_f[\varepsilon_b + (1-\varepsilon_b)\varepsilon_p]^2} \quad (22)$$

Thus, the contribution of axial dispersion and pore diffusion to the HETP can be found by subtracting Eq. (22) from Eq. (21),

$$\text{HETP}^{\#} = \text{HETP} - \text{HETP}_f = \frac{2\varepsilon_b D_b}{u_0} + \frac{2\varepsilon_p(1-\varepsilon_b)R_p^2 u_0}{15 D_p[\varepsilon_b + (1-\varepsilon_b)\varepsilon_p]^2} \quad (23)$$

Axial dispersion involves molecular diffusion and eddy diffusion. But the contribution of molecular diffusion to axial dispersion is negligible. Thus, D_b/u_0 is weakly dependent on flow velocity at low Reynolds numbers. A plot of (HETP$^{\#}$) versus u_0 in this case should give a straight line. Under these conditions, the pore diffusivity can be determined from the slope of this line, while the axial dispersion coefficient can be estimated from the intercept. One can compare measured values of the axial dispersion coefficient to those estimated from a widely used correlation given by Gunn [23]. For a well-packed column, the Gunn's correlation is given by,

$$\frac{D_b}{2R_p u} = \frac{ReSc}{4\alpha_1^2(1-\varepsilon_b)}(1-p)^2 + \frac{Re^2Sc^2}{16\alpha_1^4(1-\varepsilon_b)^2}p(1-p)^3 \times (e^{-4\alpha_1^2(1-\varepsilon_b)/p(1-p)ReSc} - 1) + \frac{\varepsilon_b}{\tau_b ReSc} \quad (24)$$

where

$$p = 0.17 + 0.33\,e^{-24/Re}, \quad \alpha_1 = 2.405, \tau_b = 1.4$$

As described in detail in the experimental section of this paper, the total bed porosity (ε_t) was determined from the first moment of pulses of SEB introduced into a column filled with resin without the affinity ligand (unretained conditions). The interstitial porosity (ε_b) was determined from the first moment of pulses of blue dextran introduced into a column filled with a resin of similar particle size to the affinity resin, but with a much smaller pore size so that blue dextran was excluded from the pores. Once the total bed porosity and the interstitial porosity were known, the particle porosity (ε_p) was calculated from Eq. (19).

From the slope and intercept of plots of HETP$^{\#}$ versus superficial velocity for SEB pulses introduced into a column with no ligand (unretained conditions) it was possible to estimate both the pore diffusivity (D_p) and the axial dispersion coefficient (D_b). The HETP$^{\#}$ values were calculated from the first and second moments of SEB pulses under unretained conditions (no ligand on the resin) according to Eqs. (21)–(23). The experimental results for axial dispersion were compared to estimates based on Gunn's correlation, Eq. (24). The film mass transfer coefficient was not determined experimentally, but was estimated from the correlation described in Eq. (20). The bi-Langmuir isotherm parameters, maximum capacities (Q_m^*) and dissociation constants (K_d), were determined from batch experiments.

Once all these mass transfer and isotherm parameters were known, the adsorption rate constants (k_a) remained the only unknown parameters since the desorption rate constants (k_d) are related to the adsorption rate constant by the equilibrium dissociation constant. The adsorption rate constants were determined from a nonlinear regression fit of the experimental breakthrough curves for SEB with the affinity resin (retained conditions).

2.4. Number of transfer units (NTU)

One way to determine the rate-limiting steps in a chromatography process is to calculate the number of transfer units of each mass transfer and surface-binding steps. The NTU is related to the HETP by the expression [24],

$$\text{NTU} = \frac{2L}{\text{HETP}}\left(\frac{k_i^{\#}}{1+k_i^{\#}}\right)^2 \quad (25)$$

where $k_i^{\#}$ is the retention factor given by $k_i^{\#} = (1-\varepsilon_b)(\varepsilon_p + K_i)/\varepsilon_b$; K_i is the equilibrium constant for adsorption, and in the absence of adsorption, it is equal to zero. LeVan et al. [24] also provide an expression for the NTU for each step in the adsorption process,

$$\text{Film mass transfer}: \; N_f = \frac{3(1-\varepsilon_b)k_f L}{R_p u \varepsilon_b} \quad (26)$$

$$\text{Pore diffusion}: \; N_p = \frac{15 D_p L}{R_p^2 u}\frac{\varepsilon_p(1-\varepsilon_b)}{\varepsilon_b} \quad (27)$$

$$\text{Axial dispersion}: \; N_d = \frac{uL}{D_b} \quad (28)$$

$$\text{Surface adsorption on site I}: \; N_{k,1} = \frac{k_{a,1}(1-\varepsilon_t)Q_{m,1}^* L}{u\varepsilon_b} \quad (29)$$

$$\text{Surface adsorption on site II}: \; N_{k,2} = \frac{k_{a,2}(1-\varepsilon_t)Q_{m,2}^* L}{u\varepsilon_b} \quad (30)$$

Note that the NTU for each step is proportional to the corresponding transfer rate coefficient. The mass transfer resistance for each step is proportional to the reciprocal of the mass transfer coefficient, and therefore proportional to the reciprocal of the NTU. The steps with the smallest number

of transfer units are rate-limiting steps and therefore control the adsorption process. The numerical values of the NTU for each transfer rate step were determined by evaluating Eqs. (26)–(30) using the previously estimated mass transfer parameters and adsorption–desorption rate constants as described previously.

3. Experimental

3.1. Synthesis of peptide resins

Peptides YYWLHH were synthesized directly onto Toyopearl AF Amino 650M (TA650M) resins (Tosoh Bioscience, Montgomeryville, PA, USA) using standard fluorenylmethyloxycarbonyl (Fmoc) chemistry as described by Buettner et al. [25]. The methacrylate-based resins have an average particle size of 65 μm with a 1000 Å average pore diameter. The aminated amino resins were modified with an alanine residue prior to peptide synthesis. To control the peptide density to final substitution levels from 6 to 220 μmol peptide/g resin, a mixture of Fmoc-L-Alanine and *tert*-butyloxycarbonyl (tBoc)-L-Alanine was coupled to the aminated resins as described by Buettner et al. [26]. The tBoc group was released with trifluoroacetic acid (TFA) and the free amino functionality was acetylated with acetic anhydride. No further peptide synthesis occurred at these acetylated sites. Subsequently, the Fmoc protecting groups were released with piperidine and the free L-Alanine was used to attach Fmoc-protected amino acids until the last cycle was finished.

3.2. Adsorption isotherm measurements

Adsorption isotherms were measured in a set of batch experiments at 20 °C. 0.5 ml centrifugal filters with 0.45 μm Durapore membranes (Millipore, Milford, MA, USA) were used as adsorption vessels. Resins (10 mg resins in each vessel) were equilibrated for at least 1 h in 400 μl of binding buffer, 0.5 M NaCl in phosphate buffer saline (PBS), pH 7.4, purchased from Sigma Chemical (St. Louis, MO, USA). After draining by centrifugation, 400 μl of SEB solution with concentrations ranging from 0.09 to 1.80 mg/ml in binding buffer were added to the reaction vessel and incubated by using an orbital shaker for 2 h. The unbound SEB was collected by centrifugation and the amount of unbound SEB was determined by Micro-BCA Assay (Pierce, Rockford, IL, USA). The amount of bound SEB was calculated by mass balance. Each isotherm measurement was made in triplicate. The amount of bound protein in the isotherm data measured in batch experiments was accurate to ±1 mg/g of resin.

3.3. Pulse experiments

The base resin, deprotected Fmoc-ala (acetyl) TA650M resin without peptides, cannot retain SEB (data not shown), and hence it was used to estimate the mass transfer properties of SEB. The TA650M resins were packed into a metal-free PEEK-lined column (4.6 mm × 15 cm I.D.) from Alltech (Deerfield, IL, USA) based on manufacturer's instructions (Tosoh Biosep, Montgomeryville, PA, USA). The pulse experiments were carried out using a Waters 616 LC system (Millipore, Milford, MA, USA) with a UV detector (Knauer, Germany) and a 50 μl sample loop (Thomson, Springfield, VA, USA). Highly purified SEB was purchased from Toxin Technology (Sarasota, FL, USA). The concentration of SEB was set at 1.5 mg/ml in the binding buffer (PBS + 0.5 M NaCl). The flow rates were 0.1, 0.2, 0.3, 0.4, 0.5 ml/min, which corresponded to superficial velocities in the column of approximately 0.01, 0.02, 0.03, 0.04, 0.05 cm/s. To account for extra-column contributions to the first moments and HETP, pulse injections of SEB were made under the same conditions with the column off-line. The first moment or HETP results with the column off-line were then subtracted from those obtained with the column on-line. It was impossible to find a void volume marker that could be excluded from the relatively large 1000 Å pore size of TA650M resin to allow measurement of the external void fraction. A column packed with HW-40C Toyopearl resin (Tosoh Biosep, Montgomeryville, PA, USA) which has a pore size of 50 Å and an average diameter of 75 μm was employed to determine the first moments using blue dextran (Sigma, St. Louis, MO, USA). The resulting interstitial porosity was used to approximate the interstitial porosity of the column with the TA650M resin. All pulse experiments were conducted at 20 °C. Each measurement was made in triplicate. The accuracy of the concentration pulse measurements taken with the HPLC is easily with in ±0.5%.

The first moment was calculated numerically using exported raw data from HPLC software,

$$\mu_1 = \frac{\sum_i C(L, t_i) t_i \Delta t}{\sum_i C(L, t_i) \Delta t} \tag{31}$$

The HETP of the pulse response can be estimated from the moment theory using Eq. (21). If pulses are not Gaussian and exhibit large amounts of tailing, it can be difficult to use this method to determine accurate second moments. However, if the chromatography peak is a Gaussian peak, the HETP can also be evaluated using the width of the peak at half-height,

$$\text{HETP} = \frac{\mu_2^* L}{\mu_1^2} = \frac{L}{5.54}\left(\frac{t_{w,0.5}}{t_r}\right)^2 \tag{32}$$

where the first absolute moment (μ_1) is identical to the retention time (t_r) of the Gaussian peak, and the second central moment (μ_2^*) is proportional to square of the peak width at half-height of the Gaussian peak by a factor 1/5.54 [27]. All the pulse responses under unretained conditions were Gaussian, so that it was possible to determine the HETP using the width at half-height formula already built into the HPLC software package. Checks were made using the direct second moment calculations by transporting the data from the HPLC

unit to a computer. The two approaches gave results for pore diffusivities within 2% of each other.

3.4. Measurement of breakthrough curves

Synthesized resins were packed into a metal-free PEEK-lined column (2.1 mm × 30 mm I.D.) from Alltech (Deerfield, IL, USA) in order to minimize the amount of SEB used. The experiments to construct the breakthrough curves were carried out at 20 °C using the same HPLC system described above. The column was pre-equilibrated with the binding buffer (0.5 M NaCl + PBS). 0.25 mg/ml of SEB in the binding buffer was loaded into a 10 ml loop (Thomson, Springfield, VA, USA) and delivered to the column at a flow rate of 0.1 ml/min. The breakthrough curve was recorded on-line by UV measurement. Samples were also collected at the exit of the column and the concentration of SEB was determined by Micro-BCA assay (Pierce, Rockford, IL, USA), as described previously in the section on isotherm measurements. The volume of each sample taken was 50 μl. Both UV traces and Micro-BCA assays gave identical results for the breakthrough curves, with a difference of no more than 1% between concentrations generated with the two methods (data not shown). The bound SEB was eluted by 2% acetic acid and then the column was regenerated with ∼50 column volumes of binding buffer. The maximal capacity of the column decreased slightly after ∼10 runs, but remained at least 95% of the original value that was obtained from the batch isotherm experiments.

4. Results and discussion

4.1. Moment and HETP analysis

The analysis of the first moments gives an accurate estimation of the total porosity of the column even if the elution profile is not a Gaussian peak, while the application of the HETP equation requires a Gaussian peak [19–21]. As seen in Fig. 1, a typical chromatogram of SEB under unretained conditions on acetyl TA650M exhibits only a small amount of tailing in comparison with the Gaussian fit. As a result, there is no question that the HETP method can be used for the determination of mass transfer parameters. The total porosity of the column was determined to be 0.787 from the slope of the first moment plot shown in Fig. 2a. Because the pore size of Toyopearl resins (1000 Å) is big enough to hold molecules up to 5 MDa in size, the widely used void volume marker, blue dextran (Mw 2 MDa), cannot be used to determine the interstitial porosity of such a column. Alternatively, a size-exclusion Toyopearl resin, HW-40C, which has the same backbone polymer and a similar particle size but much smaller pore size (50 Å) than the TA650M resin, was packed into a same column. The void fraction (interstitial porosity) of the column was determined to be 0.29 from the first moment analysis using blue dextran in pulse injections (Fig. 2a). The particle porosity was then calculated to be 0.70 by Eq. (19). The interstitial porosity (0.29) is slightly lower than with other polymer beads with similar particle size, such as agorose and sepharose beads, which lead to interstitial porosity in the range of 0.3–0.4 in well-packed columns [20,21,28].

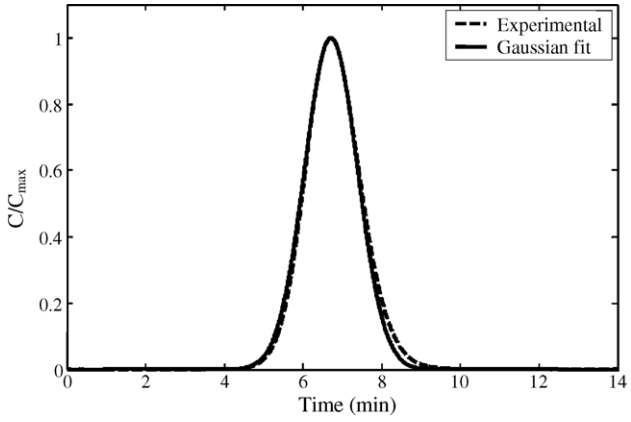

Fig. 1. Gaussian fit to experimental peak profile under unretained conditions, dashed line: experimental data on acetyl TA650M, solid line: Gaussian fit. Flow rate: 0.3 ml/min.

Having the porosities and film mass transfer coefficients calculated from Eq. (20), the axial dispersion coefficient and pore diffusivity can be determined from the intercept and slope of the HETP line respectively in Fig. 2b. The estimated pore diffusivity of SEB is 4.83×10^{-11} m^2/s. Compared to the molecular diffusivity (D_m) of SEB (7.70×10^{-11} m^2/s) [29], the diffusion of SEB inside the pores of TA650M resins is not restricted as much as other proteins with similar size to SEB in an agarose matrix [28]. This is mainly because the

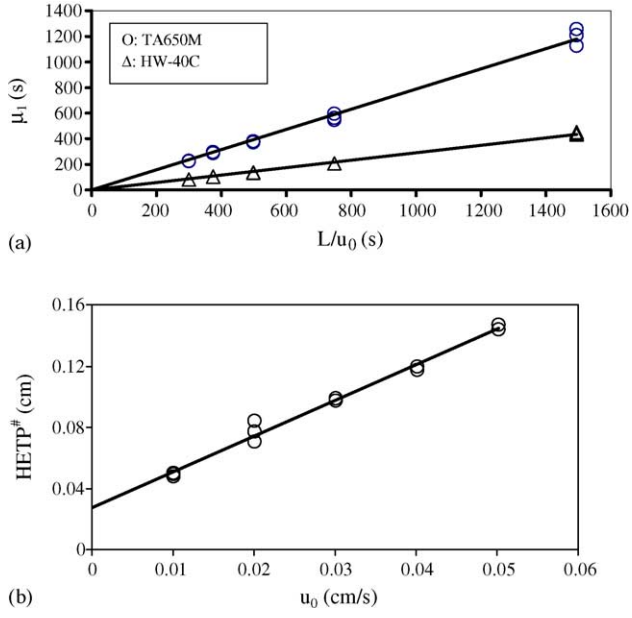

Fig. 2. (a) First moments of chromatography peaks under unretained conditions on acetyl TA650M. (b) HETP plots under unretained conditions.

large pore size of TA650M resins reduces the pore diffusion resistance. The pore diffusivity is related to the molecular diffusivity by the hindrance parameter (K_p) and the particle tortuosity factor (τ_p),

$$D_p = \frac{K_p D_m}{\tau_p} \tag{33}$$

The hindrance parameter (K_p) is related to λ_m, the ratio of the diameter of the diffusing molecule, d_m, to the pore diameter, d_{pore}. K_p can be estimated using the expression derived by Anderson and Quinn [30] when λ_m is less than 0.4 for a spherical molecule in a cylindrical pore,

$$K_p = (1-\lambda_m)^2(1-2.104\lambda_m+2.089\lambda_m^3-0.948\lambda_m^5) \tag{34}$$

The SEB molecule has dimensions of 50 Å × 45 Å × 34 Å [31], which give an equivalent diameter of 42.45 Å if the ellipsoidal molecule is treated as being spherical. The mean pore diameter of the Toyopearl amino resin is 1000 Å. This gives a value of λ_m equal to 0.043, and a hindrance parameter (K_p) equal to 0.835 according to Eq. (34). There are several empirical equations for the particle tortuosity in the literature [13,32,33]. The expression developed by Wakao and Smith [32] can be used to estimate the particle tortuosity in the TA650M resin,

$$\tau_p = \frac{1}{\varepsilon_p} \tag{35}$$

Using the measured value of $\varepsilon_p = 0.70$ for this resin, this gives a tortuosity of 1.43. Knowing the hindrance parameter and the particle tortuosity from these empirical expressions, the pore diffusivity can be estimated to be 4.50×10^{-11} m^2/s based on Eq. (33), a value which is within 7% of the measured value (4.83×10^{-11} m^2/s) using the HETP method. The value of the axial dispersion coefficient estimated from the HETP method at a flow rate of 0.3 ml/min (1.42×10^{-7} m^2/s) was also very close to that obtained from Gunn's correlation (1.42×10^{-7} m^2/s).

The GR model using the estimated mass transfer parameters was used to fit SEB pulse peaks and breakthrough curves at the end of the column under unretained conditions, with no affinity ligand on the resin. Because there is no protein bound to the stationary phase in this case, the spreading of the pulses or breakthrough curves are only due to mass transfer effects (convective mass transfer, dispersion and intraparticle diffusion). As seen in Fig. 3, the difference in spreading between the GR model predictions and the measurements under unretained conditions is inconsequential, a clear sign that all mass transfer resistances have been adequately estimated.

4.2. Equilibrium and dynamic studies of SEB adsorption

The equilibrium and dynamic behavior of SEB binding to the peptide (YYWLHH) support were thoroughly studied at a peptide density of 100 μmol/g. Accurate isotherm constants are critical to the accuracy of model calculations. Both the Langmuir equation and the bi-Langmuir equation fit the isotherm data well although the bi-Langmuir fit is better than the Langmuir fit. Fig. 4 shows the bi-Langmuir fit to the experimental data. The dissociation constants (K_d) and max-

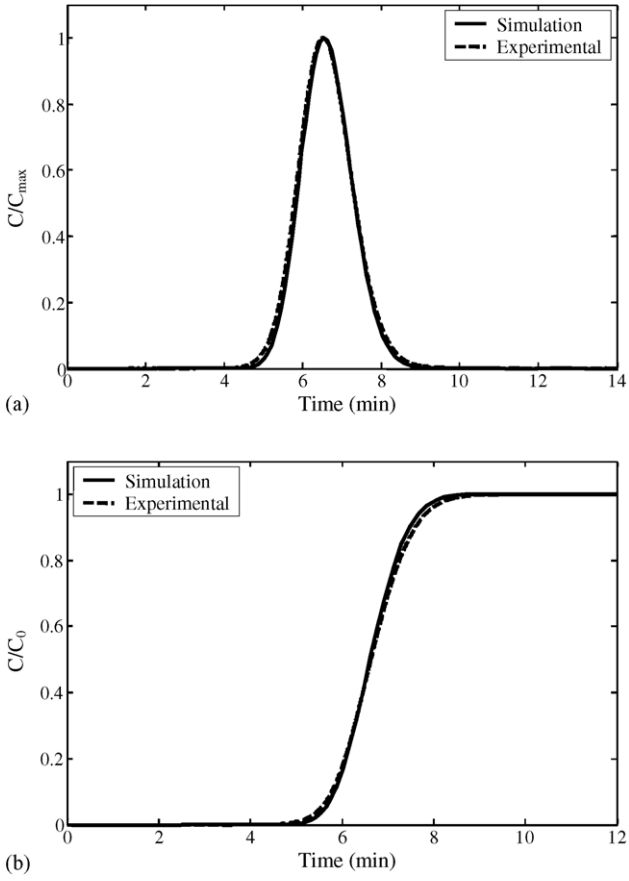

Fig. 3. Comparison of simulation (general rate model using mass transfer parameters determined from HETP equation) and experimental results under unretained conditions on acetyl TA650M. (a) A pulse injection. (b) A breakthrough curve. Flow rate: 0.3 ml/min.

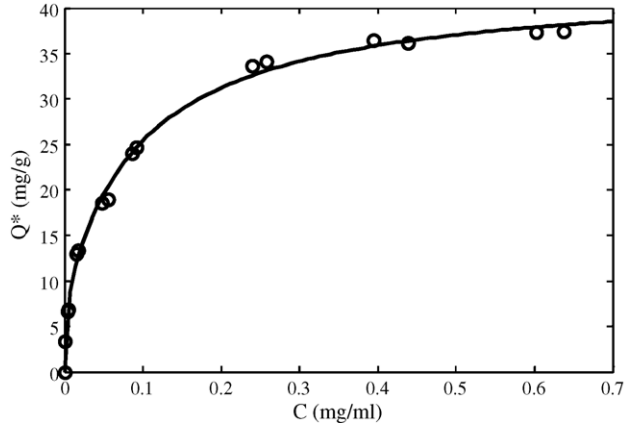

Fig. 4. The bi-Langmuir isotherm for SEB binding to YYWLHH on TA650M at a density of 100 μmol/g resin. The symbol represents experimental data, and the solid line represents the bi-Langmuir fit.

Table 1
Parameters used in the general rate model for SEB adsorption on YYWLHH at the density of 100 μmol/g in Fig. 5a

Parameter	Definition	Value
L	Column length	0.03 m
R_c	Column radius	1.05×10^{-3} m
R_p	Particle radius	32.5×10^{-6} m
C_0	Inlet concentration	9.05×10^{-3} mol/m^3
Mw	SEB molecular weight	28,366
ρ	Mobile phase density	1000 kg/m^3
u_0	Superficial velocity	4.81×10^{-4} m/s
ε_b	Interparticle void fraction	0.29
ε_p	Particle Porosity	0.70
μ	Mobile phase viscosity	0.001 Pa·s
D_b	Axial dispersion coefficient	2.40×10^{-7} m^2/s
D_m	Molecular diffusion coefficient	7.70×10^{-11} m^2/s
D_p	Diffusion coefficient inside the pores	4.83×10^{-11} m^2/s
k_f	Film mass transfer coefficient	9.51×10^{-6} m/s
Q_m^*, 1	Capacity constant of type I sites	0.43 mol/m^3 (8.50 mg/g)
Q_m^*, 2	Capacity constant of type II sites	1.74 mol/m^3 (34.42 mg/g)
$K_{d,1}$	Dissociation constant of type I sites	6.75×10^{-5} mol/m^3 (1.91×10^{-3} mg/ml)
$K_{d,2}$	Dissociation constant of type II sites	3.60×10^{-3} mol/m^3 (0.10 mg/ml)
$k_{a,1}$	Adsorption rate constant on type I sites	5.95 m^3 mol^{-1} s^{-1}
$k_{a,2}$	Adsorption rate constant on type II sites	0.40 m^3 mol^{-1} s^{-1}
$k_{d,1}$	Desorption rate constant on type I sites	4.01×10^{-4} s^{-1}
$k_{d,2}$	Desorption rate constant on type II sites	1.45×10^{-3} s^{-1}
N_d	NTU of axial dispersion	207.49
N_f	NTU of film mass transfer	38.85
N_p	NTU of pore diffusion	21.23
$N_{k,1}$	NTU of adsorption on type I sites	33.96
$N_{k,2}$	NTU of adsorption on type II sites	9.35

Note: NTU, number of transfer units; flow rate: 0.1 ml/min.

imum capacities (Q_m^*) in the bi-Langmuir equation are listed in Table 1. There are two apparent binding sites for SEB on the resins, a high affinity binding site (type I) and a lower affinity binding site (type II). The type I sites have a dissociation constant of approximately 6.75×10^{-5} mol/m^3 and the type II sites have a dissociation constant that is about 50 times larger. The total maximum SEB binding capacity of the resin is approximately 42.92 mg/g ($Q_{m,1}^* + Q_{m,2}^*$). Note that the higher affinity sites I correspond to only 20% of the total capacity and the type II sites correspond to 80% of the total capacity. A monolayer of protein adsorbs at a density of approximately 2 mg/m^2 [6]. The internal surface area of the pores of the Toyopearl particles is approximately 30 m^2/g [6], so the maximum SEB binding capacity is indicative of coverage of one monolayer or less. We can formulate two rate equations using bi-Langmuir kinetics, one is for the adsorption–desorption process on the high-energy binding site (type I site, Eq. (5)), the other is for the adsorption–desorption process on the low-energy binding site (type II site, Eq. (6)). These are used to model the breakthrough curves under adsorptive conditions.

The GR model was used to study the dynamic adsorption of SEB on YYWLHH at a density of 100 μmol/g in a chromatographic column. In order to reduce the amount of toxin, a small column with dimensions of 2.1 mm × 30 mm I.D. was used. The interstitial porosity and particle porosity of this small column were checked to make sure they were the same as in the column for the estimation of mass transfer parameters. Table 1 lists the geometrical, fluid flow, and mass transfer and isotherm parameters employed in the GR model at a flow rate of 0.1 ml/min. As shown in Fig. 5a, the GR model fits the experimental results well using only the adsorption rate constants ($k_{a,1}$, $k_{a,2}$) as the fitting parameters. The values of the adsorption rate constants were estimated using a nonlinear least-squares regression to the experimental breakthrough curve. The adsorption rate constant on the type II sites ($k_{a,2}$) is at least 10 times smaller than the adsorption rate constant on the type I sites ($k_{a,1}$). The desorption rate constants ($k_{d,1}$, $k_{d,2}$) were calculated using the equation,

$$k_d = K_d k_a \tag{36}$$

Recall that the type II sites have the largest capacity when compared to those of type I sites as shown in Table 1.

The analysis of number of transfer units described in the theory section gives the relative contributions of mass transfer steps and intrinsic adsorption rates for this particular peptide density. As shown in Table 1, the NTU for axial dispersion is significantly larger than the others (>200). Thus, axial dispersion has little influence on the adsorption rate. If axial dispersion is neglected, that is, setting the Peclet number (*Pe*) to be infinite in the GR model, the simulation is almost unchanged as shown in Fig. 5a. The NTU values for convective film mass transfer, intraparticle diffusion and adsorption rate shown in Table 1 are all in a relatively narrow range from 9 to 39, indicating that these steps all play a significant role in controlling the rate of adsorption of protein to the resin

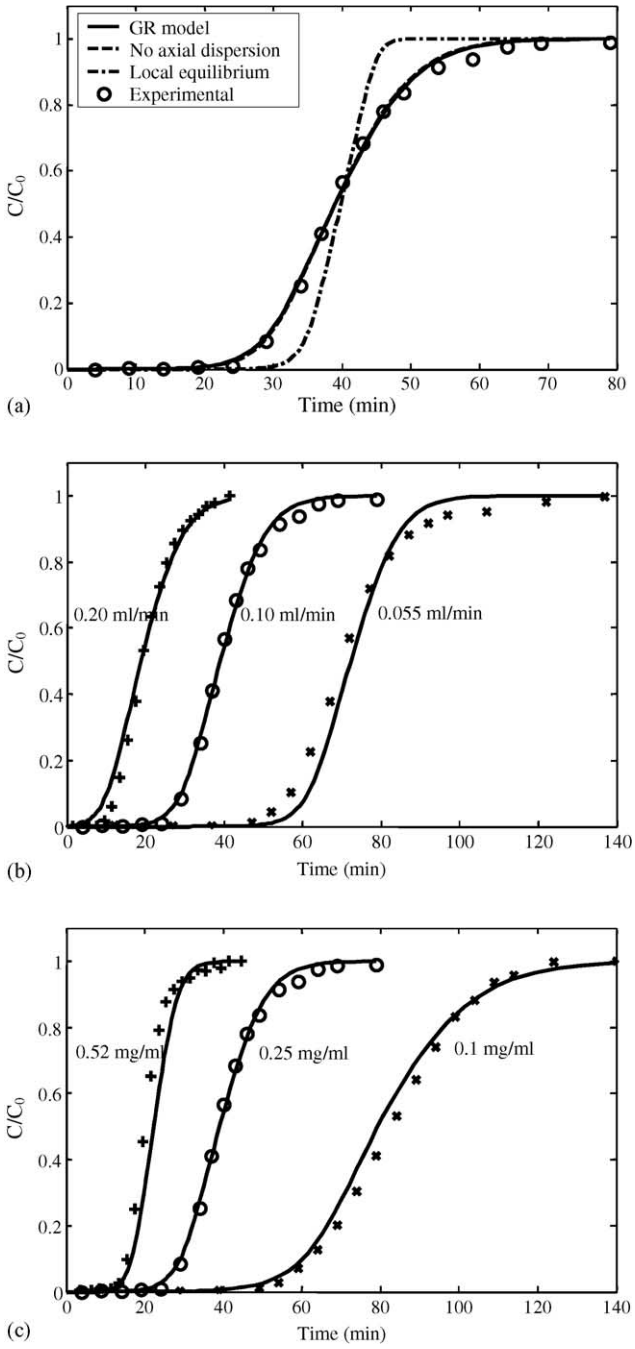

Fig. 5. Experimental (symbols) vs. simulated (lines) breakthrough curves using the GR model for SEB binding to YYWLHH on TA650M at a density of 100 μmol/g resin. (a) At base case. (—) GR model, (- - -) GR model only considering the rate-limiting steps, (–·–) GR model with the local equilibrium. Feed concentration: 0.25 mg/ml, flow rate: 0.1 ml/min. (b) At different flow rates. (+) 0.2 ml/min, (◯) 0.1 ml/min, (×) 0.055 ml/min. Feed concentration: 0.25 mg/ml. (c) At different feed concentrations. (+) 0.52 mg/ml, (◯) 0.25 mg/ml, (×) 0.10 mg/ml. Flow rate: 0.1 ml/min.

at this particular peptide density of 100 μmol/g. As seen in Fig. 5a, if we assume local equilibrium holds, that is, setting the Damkolher number for adsorption (Da^a) to be infinite in the GR model, the simulation cannot match the experimental data. Thus, our results confirm previous findings that the adsorption–desorption rates can be a relatively slow process in affinity chromatography for proteins [34,35]. As will be explained subsequently, the peptide density can play a significant role in the rate of adsorption so that the relative contributions of film mass transfer, intraparticle diffusion and adsorption to the overall rate of protein binding can change when resins have different peptide densities.

The breakthrough curves also can be predicted properly by the GR model at different flow rates (Fig. 5b) and inlet concentrations of SEB (Fig. 5c). The film mass transfer coefficient and axial dispersion coefficient depend on the flow velocity, and these were adjusted based on Eqs. (20) and (24), respectively in doing calculations at different flow velocities. The pore diffusivity and rate constants remained the same in these simulations. It has been demonstrated that surface diffusion plays an important role in reverse phase liquid chromatography [36]. If surface diffusion played an equally important role in peptide affinity chromatography, one would expect an experimental breakthrough curve that is much steeper than the model predictions at low inlet concentrations, e.g. 0.1 mg/ml. As shown in Fig. 5c, the agreement between the experimental and simulated breakthrough curves confirms the assumption of neglecting surface diffusion when the GR model was formulated in our analysis.

Several simple models including the lumped pore diffusion model, transport-dispersive model and reaction-dispersive model have been compared to the GR model. The formulation of these models is in the Appendix. The POR model considers all mass transfer effects like the GR model but greatly reduces the mathematical complexity. If the pore diffusivity is not too small, the POR model could give a prediction that is as good as the GR model [8]. As seen in Fig. 6a, the results of the POR model considering proper adsorption–desorption kinetics are almost identical to those of the GR model and provide a good fit to the experimental breakthrough curve. If we assume local equilibrium exists, which is a general assumption in ion-exchange and reverse phase chromatography, the simulated breakthrough curve becomes steeper leading to mismatch with the experimental data. The TD model with “solid film” driving force fails to model the breakthrough curve because it cannot take into account properly the adsorption–desorption kinetics, which is one of the major rate-limiting steps (Fig. 6b). The failure of the RD model shown in Fig. 6c is because it neglects film mass transfer and pore diffusion. The RD model might be improved using the lumped rate constants (Eq. (C.4)) that include film mass transfer coefficient and pore diffusivity in addition to the intrinsic rate constants [20]. As seen in Fig. 6c, the lumped adsorption rate constants are too small so that the simulation deviates from the experimental data. This indicates that the influences of the film mass transfer and pore diffusion are comparable to those of the adsorption–desorption rates. The RD model is best to model chromatographic processes in which the intrinsic adsorption–desorption step is the only rate-limiting step, so the RD model with the lumped rate parameters does not do well in this case. The success of the

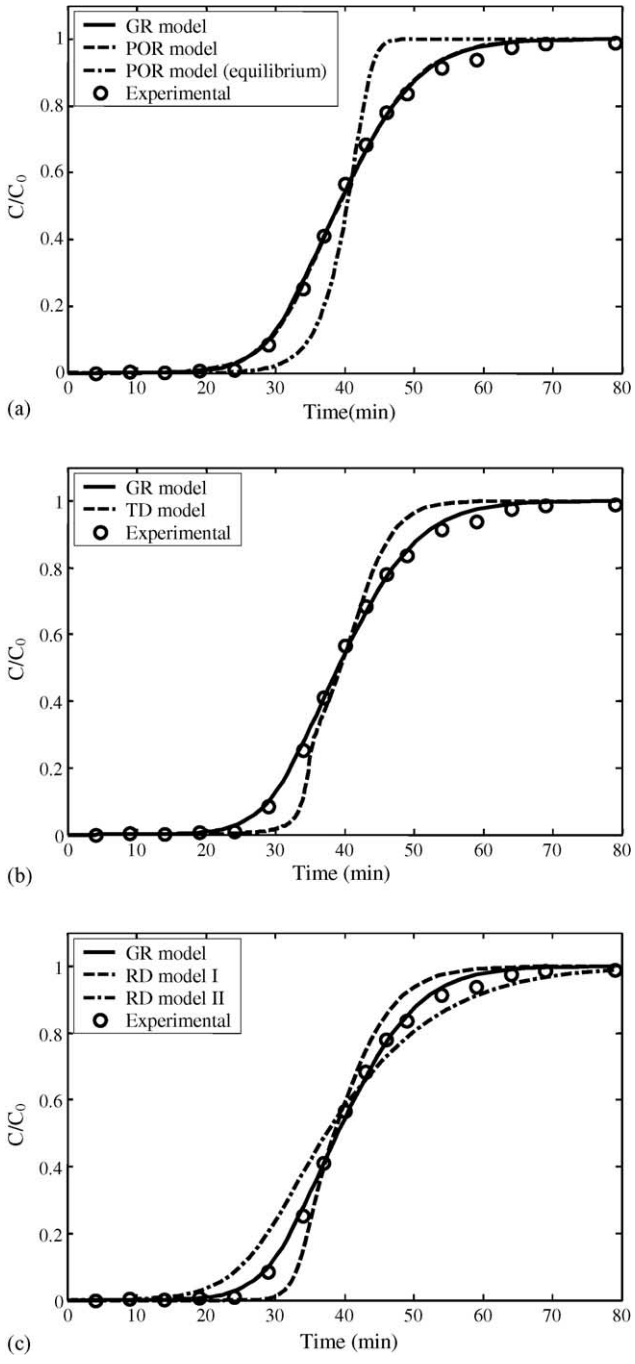

Fig. 6. (a) Comparison between the POR model and the GR model. (◯) Experimental data, (—) GR model, (- - -) POR model, (–·–) POR model with local equilibrium. (b) Comparison between the TD model and the GR model. (◯) Experimental data, (—) GR model, (- - -) TD model. (c) Comparison between the RD model and the GR model. (◯) Experimental data, (—) GR model, (- - -) RD model with the intrinsic rate parameters (RD model I), (–·–) RD model with the lumped rate parameters (RD model II). Flow rate: 0.1 ml/min, feed concentration: 0.25 mg/ml, YYWLHH on TA650M at a density of 100 μmol/g resin.

GR and POR models and the failure of the TD and RD models further confirm the conclusion from the NTU analysis, that is, both film and intraparticle mass transfer and surface adsorption–desorption rates are rate-limiting.

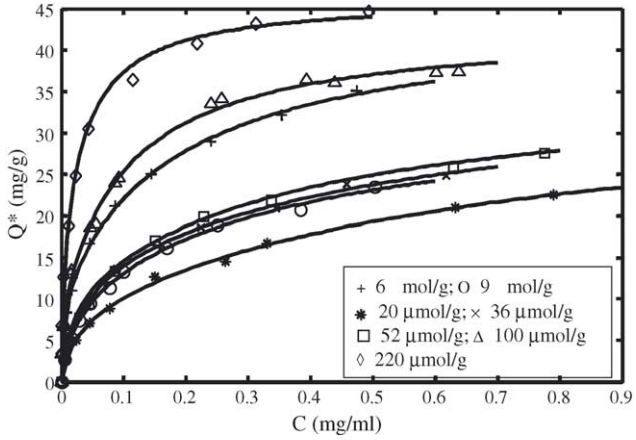

Fig. 7. Isotherms for SEB binding to YYWLHH on TA650M at different peptide densities. The symbol represents experimental data, and the solid line represents the bi-Langmuir fit.

4.3. Effect of peptide density on SEB adsorption

The measured SEB adsorption isotherms on Toyopearl 650M resin with different peptide densities are shown in Fig. 7. Each isotherm was fitted to both the bi-Langmuir and the Langmuir equation by nonlinear least-squares regressions. It was found that the bi-Langmuir equation fit the equilibrium data ($R^2 \geq 0.99$) better than the Langmuir equation ($R^2 \approx 0.96$) especially at high concentrations of SEB. Only the bi-Langmuir fits are shown in Fig. 7. The results of dissociation constants (K_d), maximum capacities (Q_m^*) and correlation coefficients (R^2) for the bi-Langmuir fitting are listed in Table 2 for the different peptide densities.

The effects of peptide density on the dissociation constant and maximum capacity of the various resins with different peptide densities are shown in Fig. 8. Fig. 8a indicates that the dissociation constants at low peptide density are low, increase with increasing peptide density to a maximum value, and then decrease to reach a nearly constant value with increasing peptide density. This indicates that the binding affinity of SEB to this peptide resin is high at very low peptide density, and then decreases with increasing density, followed by another increase at high peptide density. There is a sudden decrease in the binding capacity when the peptide density increases from 6 to 9 μmol/g, followed by an increase in the maximum capacity as the peptide density increases (Fig. 8b). As shown in Fig. 8b, the total maximum capacity of each resin is less than 50 mg/g. Given that the internal area surface area of the Toyopearl Amino 650M resin is approximately 30 m^2/g and that a monolayer of protein contains approximately 2 mg of protein/m^2, this indicates that for this range of peptide densities the coverage of SEB on the surface of the resin is less than or equal to a monolayer.

SEB is shaped like an ellipsoid with dimensions of 50 Å × 45 Å × 34 Å [31]. It covers an area of approximately 1415 $Å^2$. Using this information, and estimating the surface area for binding to the resin to be 30 m^2/g, the number of

Table 2
Isotherm parameters at different peptide densities

	Units	Peptide (μmol/g)						
		6 8.68[a]	9 13.02[a]	20 28.93[a]	36 52.08[a]	52 75.23[a]	100 142.86[a]	220 318.26[a]
$Q^*_{m,1}$	(mg/g)	11.47	9.31	8.07	13.74	10.49	8.50	13.94
	(mol/m^3)[b]	0.56	0.48	0.41	0.70	0.54	0.43	0.71
$Q^*_{m,2}$	(mg/g)	32.86	24.35	27.30	23.65	25.78	34.42	33.26
	(mol/m^3)[b]	1.68	1.24	1.39	1.21	1.32	1.74	1.70
$K_{d,1}$	(mg/ml) × 10^3	5.80	19.12	22.95	29.60	15.06	1.91	1.56
	(mol/m^3) × 10^4	2.04	6.74	8.09	10.43	5.31	0.68	0.55
$K_{d,2}$	(mg/ml)	0.19	0.36	0.68	0.60	0.38	0.10	0.047
	(mol/m^3) × 10^3	6.84	12.80	23.92	21.19	13.26	3.60	1.67
R^2	Correlation coefficient	0.998	0.998	0.998	0.999	0.998	0.997	0.998

Note: the bulk density of resins is 320 ± 4 mg/ml.
[a] Density (mol/m^3).
[b] Based on unit volume of particle skeleton.

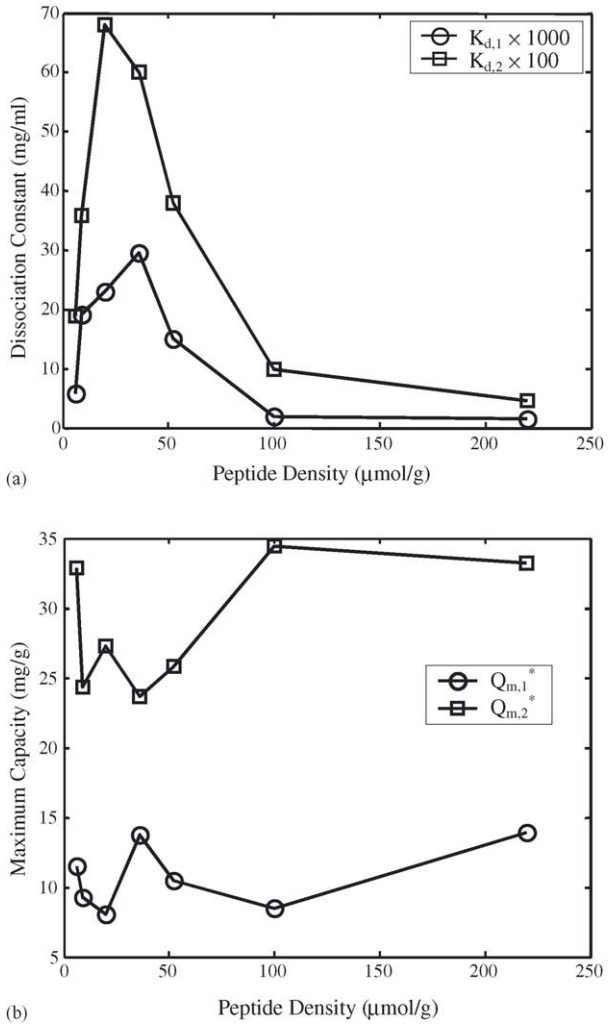

Fig. 8. (a) Variation of dissociation constant for SEB adsorption to YYWLHH on TA650M with different peptide densities. (b) Variation of maximum capacity for SEB adsorption to YYWLHH on TA650M with different peptide densities.

peptides covered by one SEB molecule at different peptide densities was calculated (Table 3). At low peptide density, the interactions between SEB molecules and peptides are approximately monovalent and are probably bio-specific. Increases in ligand density from low values apparently introduce steric hindrances for further protein binding so that the affinity of the ligands tends to decrease and hence the dissociation constant increases. After the peptide density reaches a certain level, the adsorption mechanism may switch to multivalent interactions from monovalent interactions. The multivalent interaction is a combination of specific and nonspecific interactions between the protein and several peptides. In this case, the interactions between SEB molecules and peptides are strengthened and hence the dissociation constant decreases with increasing ligand density. The transition of the binding mechanism can also explain the variation in the maximum capacity with peptide density. For single point and bio-specific binding, the increase in peptide density introduces more steric hindrances for SEB binding, and therefore causes the maximum capacity to decrease. If the binding mechanism switches to multipoint binding, the maximum capacity typically increases with increases in peptide density. The transition zone of peptide density in which the SEB adsorption process changes from monovalent binding to multivalent binding is in the range from 9 to 36 μmol/g as shown in Fig. 8. When the peptide density is

Table 3
Surface area estimates

Peptide density (μmol/g)	Number of peptides covered by one SEB molecule
6	1.7
9	2.6
20	5.7
36	10.2
52	14.8
100	28.4
220	62.5

Table 4
Adsorption rate constants at different peptide densities

	Peptide density (μmol/g)						
	6	9	20	36	52	100	220
$k_{a,1}$ ($m^3\,mol^{-1}\,s^{-1}$)	1.24	1.14	0.60	0.45	1.02	5.95	9.11
$k_{d,1}$ (s^{-1}) × 10^4	2.52	7.67	4.85	4.70	5.43	4.01	5.02
$k_{a,2}$ ($m^3\,mol^{-1}\,s^{-1}$)	0.36	0.14	0.32	0.19	0.13	0.40	0.50
$k_{d,2}$ (s^{-1}) × 10^4	24.6	18.03	75.65	40.64	17.74	14.54	8.33

no less than 52 μmol/g, the total maximum capacity remains constant with a value of ∼44 mg/g, and increases in peptide density show little effect on the total maximum capacity as shown in Table 2. This is probably because the surface of the affinity support has already been completely occupied by a monolayer of SEB. Under these conditions, the ratio of the number of peptides to SEB molecules bound keeps increasing (Table 3) and the dissociation constant keeps decreasing (Table 2). This indicates that, under conditions of multi-point interaction between peptide ligands and SEB, increases in peptide density lead to increased interactions with the surface.

The dynamic behavior of SEB binding to YYWLHH on resins with different peptide densities was studied experimentally using frontal chromatography. The breakthrough curves are shown in Fig. 9. The GR model was used to fit the adsorption rate constant for all these curves using bi-Langmuir kinetics. As shown previously, the adsorption rate constants were obtained using a nonlinear least-squares regression to fit the breakthrough curve, and the desorption rate constants were calculated by Eq. (36). All the resulting rate constants at different peptide densities are listed in Table 4. In comparison with Table 2, it can be seen that smaller dissociation constants, which indicate higher affinity, are associated with larger adsorption rate constants. The bi-Langmuir kinetics results show an increase in the adsorption rate constants with increasing peptide density on the type I binding sites, and no clear trend of adsorption rate constants with peptide density

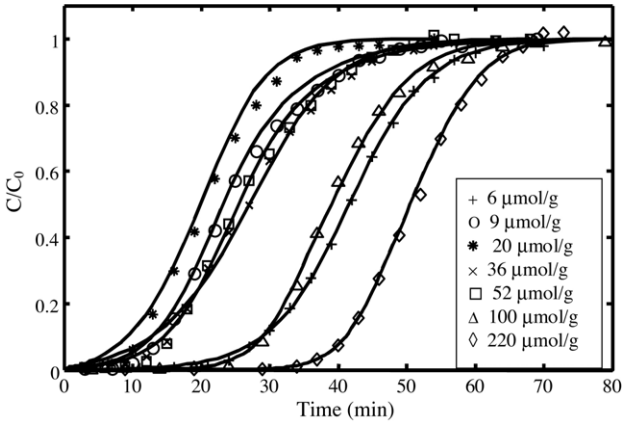

Fig. 9. Experimental (symbols) vs. simulated (lines) breakthrough curves using the GR model at different peptide densities. Flow rate: 0.1 ml/min, feed concentration: 0.22 mg/ml for resins with a density of 6 μmol/g, 0.25 ± 0.1 mg/ml for others.

Table 5
Number of mass transfer units at different peptide densities

	Peptide density (μmol/g)						
	6	9	20	36	52	100	220
N_d	207.49	207.49	207.49	207.49	207.49	207.49	207.49
N_f	38.85	38.85	38.85	38.85	38.85	38.85	38.85
N_p	21.23	21.23	21.23	21.23	21.23	21.23	21.23
$N_{k,1}$	9.59	7.17	3.27	4.19	7.27	33.96	86.00
$N_{k,2}$	8.01	2.31	5.84	3.07	2.34	9.35	11.23

on type II sites. These results indicate that there may be different binding mechanisms on these two kinds of sites but it is not clear what might be causing this effect.

The relative contributions of mass transfer and intrinsic adsorption rates were also investigated at different peptide densities. The number of transfer units for each mass transfer step and intrinsic adsorption rates were calculated using Eqs. (26)–(30). As shown in Table 5, the intrinsic adsorption step always has the smallest number of transfer units. Therefore, SEB adsorption on YYWLHH with various peptide densities from 6 to 220 μmol/g is adsorption-rate limited. However, film mass transfer and pore diffusion also offer significant limitations to protein binding and need to be properly considered in modeling the breakthrough curves. This is particularly well illustrated in the results with a peptide density of 100 μmol/g where the NTUs for film mass transfer, intraparticle diffusion and adsorption are all about the same order of magnitude.

5. Conclusions

The mass transfer rates and intrinsic adsorption–desorption kinetics of SEB adsorption on YYWLHH attached to TA650M resins with ligand densities from 6 to 220 μmol/g have been evaluated. The first and second moments of SEB pulses under unretained conditions were used for the estimation of the bed porosity, the interparticle porosity, the pore porosity, the axial dispersion coefficient and the pore diffusivity. Equilibrium adsorption isotherms for SEB binding to these resins were also measured to determine the variation in binding capacity and dissociation constant with peptide density. It was found that the pore diffusivity of SEB in TA650M is fairly close to the molecular diffusivity due to the large (1000 Å) average pore size of the resin. Using classical expressions for hindered diffusion and tortuosity in the pores,

it was possible to estimate a pore diffusivity value that was within 7% of the measured value.

The GR model for chromatography using the estimated mass transfer parameters was used to fit the dynamic breakthrough curves to obtain adsorption rate constants using a nonlinear least-squares regression. An analysis of the number of transfer units for the various mass transfer and adsorption kinetics steps revealed that film mass transfer, pore diffusion and intrinsic adsorption can all contribute significantly to the overall rate of adsorption of protein to the resin. A comparison of results of the GR model with simpler models such as the POR model, the TD model and the RD model, further confirmed this conclusion.

The binding capacity of the various resins was higher at low and high peptide density and exhibited a slight decrease in the range of 20–50 μmol/g. The dissociation constant at low and high peptide densities was smaller than at intermediate peptide densities. This suggests that at low peptide density, where the ratio of bound protein to peptide is close to 1/2, there is a nearly one-to-one interaction between the ligands and the protein, while in the high peptide density region, where the protein to ligand ratio is roughly 1/60, there is also a strong multipoint interaction that is likely to be less specific. The slight decrease in capacity at intermediate peptide densities is likely due to a small steric hindrance effect caused by crowding of the peptide ligands on the surface.

The breakthrough curves at different peptide densities and flow velocities were well predicted by the GR model. It was found that, especially at the lower peptide densities, the intrinsic adsorption step has the smallest number of transfer units, indicating that intrinsic adsorption is the slowest process, with film and intraparticle diffusion also providing a significant contribution to rate limitations.

6. Nomenclature

a	parameters in the dimensionless Langmuir isotherm, Q_m^*/K_d
b	parameters in the dimensionless Langmuir isotherm (C_0/K_d)
Bi	Biot number ($k_f R_p/(\varepsilon_p D_p)$)
C_0	feed concentration
C_b	concentration in the bulk phase
c_b	dimensionless concentration in the bulk phase (C_b/C_0)
C_{max}	maximum concentration at the column outlet for a pulse injection
C_p	concentration in the stagnant fluid phase inside the particle pores
c_p	dimensionless concentration in the stagnant fluid phase inside the particle pores (C_p/C_0)
$\overline{C}_p$	average concentration in the stagnant fluid phase inside the particle pores
$\overline{c}_p$	dimensionless average concentration in the stagnant fluid phase inside the particle pores $\overline{C}_p/C_0$
D_b	axial dispersion coefficient
D_m	molecular diffusion coefficient
d_m	molecule diameter
D_p	pore diffusivity ($K_p D_m/\tau_p$)
d_{pore}	pore diameter
Da^a	Damkolher number for adsorption ($Lk_a C_0/u$)
Da^d	Damkolher number for desorption (Lk_d/u)
F	phase ratio $(1-\varepsilon_t)/\varepsilon_t$
HETP	height equivalent to a theoretical plate
K	slope of isotherm chord
K_i	equilibrium constant
K_d	dissociation constant
K_p	hindrance parameter
k_a	adsorption rate constant
k_{al}	lumped adsorption rate constant
k_d	desorption rate constant
k_i	internal mass transfer coefficient
$k_i^\#$	retention factor
k_f	film mass transfer coefficient
k_m	overall mass transfer coefficient in the TD model
k_t	lumped mass transfer coefficient in the POR model
L	column length
Mw	molecular weight of SEB
N_d	number of transfer units for the axial dispersion
N_f	number of transfer units for the film mass transfer
N_k	number of transfer units for the adsorption kinetics
N_p	number of transfer units for the pore diffusion
p	parameter in Gunn correlation
Pe	Peclet number in the GR model and the POR model (uL/D_b)
$Pe^\#$	Peclet number in the TD model and the RD model ($u_t L/D_b$)
Q	concentration in the solid phase (based on unit volume of particle skeleton)
q	dimensionless concentration in the solid phase (Q/C_0)
Q_m^*	adsorption saturation capacity (based on unit volume of particle skeleton)
q_m^*	dimensionless adsorption saturation capacity, Q_m^*/C_0
$\overline{Q}$	average concentration in the solid phase
$\overline{q}$	dimensionless average concentration in the solid phase, $\overline{Q}/C_0$
R	radial coordinate
r	dimensionless radial coordinate (R/R_p)
R_p	particle radius
R_c	column radius
R^2	correlation coefficient
r_s	separation factor
Re	Reynolds number ($2R_p \rho u \varepsilon_b/\mu$)
Sc	Schmidt number ($\mu/(\rho D_m)$)
Sh	Sherwood number ($k_f(2R_p)/D_m$)
St	Stanton number in the GR model ($3k_f L/(R_p u)$)
$St^\#$	Stanton number in the POR model ($3k_t L/(R_p u)$)

$St^{\#\#}$ Stanton number in the TD model ($k_m L/u_t$)
t time
t_r retention time
$t_{w,0.5}$ width at half-height of a peak
u interstitial velocity (u_0/ε_b)
u_0 superficial velocity
u_t chromatographic velocity (u_0/ε_t)
Z axial coordinate
z dimensionless axial coordinate (Z/L)

Greek letters
α_1 first root of the zero-order Bessel function
ε_b interstitial porosity
ε_p particle porosity
ε_t total porosity
η dimensionless constant ($St/(3Bi)$)
λ_m ratio of molecule diameter to pore diameter (d_m/d_{pore})
μ mobile phase viscosity
μ_1 first absolute moment of peak
μ_2^* second central moment of peak
ρ mobile phase density
τ dimensionless time (tu/L)
τ_b column tortuosity
τ_p particle tortuosity
ξ dimensionless constant $(1-\varepsilon_b)St/\varepsilon_b$
$\xi^{\#}$ dimensionless constant $(1-\varepsilon_b)St^{\#}/\varepsilon_b$

Subscripts
1, 2 type I binding sites, type II binding sites
m maximum capacity

Superscripts
* equilibrium value

Acknowledgement

The authors would like to thank Dr. Patrick V. Gurgel for the helpful discussions on the effects of peptide density on protein adsorption.

Appendix A. Lumped pore diffusion (POR) model

The POR model is a simplification of the GR model and can be derived from the GR model by integrating Eq. (3) over the particle volume [37,38]. The adsorbate concentration in the mobile phase in the pores is taken as the average solute concentration in the particle. The influences of the external mass transfer (k_f) and pore diffusion (D_p) are lumped together and characterized by a lumped mass transfer coefficient (k_t). The POR model has been extensively used to describe the zone profiles and breakthrough curves in preparative liquid chromatography [8,39,40]. The formulation of the POR model in this paper is almost the same as in the literature except for the consideration of the kinetics of surface reaction,

$$\frac{\partial c_b}{\partial \tau} - \frac{1}{Pe}\frac{\partial^2 c_b}{\partial z^2} + \frac{\partial c_b}{\partial z} + \xi^{\#}(c_b - \bar{c}_p) = 0 \tag{A.1}$$

$$(1-\varepsilon_p)\frac{\partial \bar{q}}{\partial \tau} + \varepsilon_p \frac{\partial \bar{c}_p}{\partial \tau} - St^{\#}(c_b - \bar{c}_p) = 0 \tag{A.2}$$

As in the GR model, bi-Langmuir kinetics is used,

$$\bar{q} = \bar{q}_1 + \bar{q}_2 \tag{A.3}$$

$$\frac{\partial \bar{q}_1}{\partial \tau} = Da_1^a c_p(q_{m,1}^* - \bar{q}_1) - Da_1^d \bar{q}_1 \tag{A.4}$$

$$\frac{\partial \bar{q}_2}{\partial \tau} = Da_2^a c_p(q_{m,2}^* - \bar{q}_2) - Da_2^d \bar{q}_2 \tag{A.5}$$

If local equilibrium exists, then Eqs. (A.4) and (A.5) reduce to the form,

$$\bar{q}_1^* = \frac{a_1 \bar{c}_p}{1 + b_1 \bar{c}_p} \tag{A.6}$$

$$\bar{q}_2^* = \frac{a_2 \bar{c}_p}{1 + b_2 \bar{c}_p} \tag{A.7}$$

The initial and boundary conditions are similar to those used in the GR model.

The lumped mass transfer coefficient (k_t) is given by the relationship [37],

$$\frac{1}{k_t} = \frac{1}{k_f} + \frac{1}{k_i \varepsilon_p} \tag{A.8}$$

where k_i is the internal mass transfer coefficient proposed by [41],

$$k_i = \frac{5 D_p}{R_p} \tag{A.9}$$

Appendix B. Transport-dispersive (TD) model

The formulation of the TD model appears elsewhere [8,13,21]. A solid film driving force model is employed to describe the adsorption on each type of binding site when bi-Langmuir kinetics is employed,

$$\frac{\partial c_b}{\partial \tau} + F\frac{\partial q}{\partial \tau} - \frac{1}{Pe^{\#}}\frac{\partial^2 c_b}{\partial z^2} + \frac{\partial c_b}{\partial z} = 0 \tag{B.1}$$

$$q = q_1 + q_2 \tag{B.2}$$

$$\frac{\partial q_1}{\partial \tau} = St^{\#\#}(q_1^* - q_1) \tag{B.3}$$

$$\frac{\partial q_2}{\partial \tau} = St^{\#\#}(q_2^* - q_2) \tag{B.4}$$

The initial and boundary conditions are similar to those used in the GR model.

The overall mass transfer coefficient (k_m) in the solid film linear driving force model is given by the following equation [13,42],

$$\frac{1}{k_m} = \frac{K}{F}\left(\frac{R_p}{3k_f} + \frac{R_p^2}{15\varepsilon_p D_p}\right) \tag{B.5}$$

where K (the slope of the isotherm chord) is given by,

$$K = F\frac{\Delta Q^*}{\Delta C} \tag{B.6}$$

Appendix C. Reaction-dispersive (RD) model

The RD model assumes that the adsorption–desorption kinetics is the rate-limiting step [21],

$$\frac{\partial c_b}{\partial \tau} + F\frac{\partial q}{\partial \tau} - \frac{1}{Pe^{\#}}\frac{\partial^2 c_b}{\partial z^2} + \frac{\partial c_b}{\partial z} = 0 \tag{C.1}$$

$$\frac{\partial q_1}{\partial \tau} = Da_1^a c_p(q^*_{m,1} - q_1) - Da_1^d q_1 \tag{C.2}$$

$$\frac{\partial q_2}{\partial \tau} = Da_2^a c_p(q^*_{m,2} - q_2) - Da_2^d q_2 \tag{C.3}$$

If the mass transfer effects have a minor influence but cannot be neglected, a lumped adsorption coefficient (k_{al}) could replace the intrinsic adsorption coefficient (k_a) in the Damkolher number (Da^a) to account for mass transfer effects [28],

$$\frac{1}{k_{al}} = \frac{1}{k_a} + \frac{Q^*_m(1+r_s)R_p^2}{30r_s}\left(\frac{1}{\varepsilon_p D_p} + \frac{5}{k_f R_p}\right) \tag{C.4}$$

where r_s is the separation factor defined by,

$$r_s = 1 + \frac{C_0}{K_d} \tag{C.5}$$

References

[1] K. Amatschek, R. Necina, R. Hahn, E. Schallaun, H. Schwinn, D. Josic, A. Jungbauer, J. High Resolut. Chromatogr. 23 (2000) 47.
[2] P.D. Bastek, J.M. Land, G.A. Baumbach, D.H. Hammond, R.G. Carbonell, Sep. Sci. Technol. 35 (2000) 1681.
[3] P.V. Gurgel, R.G. Carbonell, H.E. Swaisgood, Bioseparation 9 (2001) 385.
[4] P.Y. Huang, R.G. Carbonell, Biotechnol. Bioeng. 47 (1995) 288.
[5] P.Y. Huang, G.A. Baumbach, C.A. Dadd, J.A. Buettner, B.L. Masecar, M. Hentsch, D.J. Hammond, R.G. Carbonell, Bioorg. Med. Chem. 4 (1996) 699.
[6] D.B. Kaufman, M.E. Hentsch, G.A. Baumbach, J.A. Buettner, C.A. Dadd, P.Y. Huang, D.J. Hammond, R.G. Carbonell, Biotechnol. Bioeng. 77 (2002) 278.
[7] K. Pflegerl, A. Podgornik, E. Berger, A. Jungbauer, Biotechnol. Bioeng. 79 (2002) 733.
[8] K. Kaczmarski, D. Antos, H. Sajonz, P. Sajonz, G. Guiochon, J. Chromatogr. A 925 (2001) 1.
[9] N. Balaban, A. Rasooly, Int. J. Food Microbiol. 61 (2000) 1.
[10] H. Li, A. Llera, E.L. Malchiodi, R.A. Mariuzza, Annu. Rev. Immunol. 17 (1999) 435.
[11] R.G. Ulrich, S. Sidell, T.J. Taylor, C.L. Wilhelmsen, D.R. Franz, in: F.R. Sidell, E.T. Takafuji, D.R. Franz (Eds.), Medical Aspects of Chemical and Biological Warfare, Office of the Surgeon General at TMM Publications, Borden Institute, Walter Reed Army Medical Center, Washington, DC, 1997, p. 621.
[12] G. Wang, J. De, J.S. Schoeniger, D.C. Roe, R.G. Carbonell, J. Peptide Res. 64 (2004) 51.
[13] G. Guiochon, S.G. Shirazi, A.M. Katti, Fundamentals of Preparative and Nonlinear Chromatography, Academic Press, Boston, 1994.
[14] P.D. Bastek, Dissertation in Chemical Engineering, North Carolina State University, Raleigh, NC, 2000.
[15] T. Gu, Mathematical Modeling and Scale-up of Liquid Chromatography, Springer, New York, 1995.
[16] P.V. Danckwerts, Chem. Eng. Sci. 2 (1953) 1.
[17] B.A. Finlayson, Nonlinear Analysis in Chemical Engineering, McGraw-Hill, New York, 1980.
[18] J. Villadsen, M.L. Michelsen, Solutions of Differential Equation Models by Polynomial Approximation, Prentice Hall, Englewood Cliff, 1978.
[19] F.H. Arnold, H.W. Blanch, C.R. Wilke, Chem. Eng. J. 30 (1985) B25.
[20] P.M. Boyer, J.T. Hsu, AIChE J. 38 (1992) 259.
[21] V. Natarajan, S.M. Cramer, Sep. Sci. Technol. 35 (2000) 1719.
[22] N. Wakao, T. Oshima, S. Yagi, Kagaku Kogaku 22 (1958) 780.
[23] D.J. Gunn, Chem. Eng. Sci. 42 (1987) 363.
[24] M.D. LeVan, G. Carta, C.M. Yon, in: R.H. Perry, D.W. Green (Eds.), Chemical Engineer's Handbook, MacGraw-Hill, New York, 1997.
[25] J.A. Buettner, C.A. Dadd, G.A. Baumbach, B.L. Masecar, D.J. Hammond, Int. J. Peptide Protein Res. 47 (1996) 70.
[26] J.A. Buettner, C.A. Dadd, G.A. Baumbach, D.J. Hammond, in US Patent, No. 5,723,579, U.S. (1997).
[27] C. Horvath, W.R. Melander, in: E. Heftmann (Ed.), Chromatography, Part A, Elsevier, Amsterdam, 1983, p. A28.
[28] P.M. Boyer, J.T. Hsu, Chem. Eng. Sci. 47 (1992) 241.
[29] J. Wagman, R.C. Edwards, E.J. Schantz, Biochemistry 4 (1965) 1017.
[30] J.L. Anderson, J.A. Quinn, Biophys. J. 14 (1974) 130.
[31] A.C. Papageorgiou, H.S. Tranter, K.R. Acharya, J. Mol. Biol. 277 (1998) 61.
[32] N. Wakao, J.M. Smith, Chem. Eng. Sci. 17 (1962) 825.
[33] M. Suzuki, J.M. Smith, Chem. Eng. J. 3 (1972) 256.
[34] A.I. Liapis, J. Biotechnol. 11 (1989) 143.
[35] A.I. Liapis, Sep. Purif. Methods 19 (1990) 133.
[36] M. Gubernak, X. Liu, K. Kaczmarski, G. Guiochon, Biotechnol. Prog. 20 (2004) 1496.
[37] M. Morbidelli, A. Servida, G. Storti, S. Carra, Ind. Eng. Chem. Fundam. 21 (1982) 123.
[38] M. Morbidelli, G. Storti, S. Carra, Chem. Eng. Sci. 39 (1984) 383.
[39] X. Liu, K. Kaczmarski, A. Cavazzini, P. Szabelski, D. Zhou, G. Guiochon, Biotechnol. Prog. 18 (2002) 796.
[40] D. Zhou, X. Liu, K. Kaczmarski, A. Felinger, G. Guiochon, Biotechnol. Prog. 19 (2003) 945.
[41] E. Glueckauf, Trans. Faraday Soc. 51 (1955) 1540.
[42] K. Miyabe, G. Guiochon, Biotechnol. Prog. 15 (1999) 740.